NANO LETTERS

Letter

pubs.acs.org/NanoLett

Impact of Surface-Bound Small Molecules on the Thermoelectric Property of Self-Assembled Ag_2Te Nanocrystal Thin Films

Yanming Sun,[†,‡] Haiyu Fang,[‡] Lujun Pan,[†] Meng Han,[§] Shen Xu,[§] Xinwei Wang,[§] Biao Xu,[∥] and Yue Wu*[,∥]

[†]School of Physics and Optoelectronic Technology, Dalian University of Technology, Dalian, Liaoning 116024, People's Republic of China

[‡]School of Chemical Engineering, Purdue University, West Lafayette, Indiana 47907, United States

[§]Department of Mechanical Engineering and [∥]Department of Chemical and Biological Engineering, Iowa State University, Ames, Iowa 50011, United States

ABSTRACT: Small molecules with functional groups can show different electron affinity and binding behavior on nanocrystal surface, which in principle could be used to alternate the electrical transport in self-assembled nanocrystal thin films. These small molecules can also serve for scattering the phonons to reduce the thermal conductivity. Here, we present our research on the thermoelectric characteristic of self-assembled silver telluride (Ag_2Te) nanocrystal thin films that are fabricated by a layer-by-layer (LBL) dip-coating process. We perform investigations on the electrical conductivity and Seebeck coefficient on the Ag_2Te nanocrystal thin films containing hydrazine, 1,2-ethanedithiol, and ethylenediamine between 300 and 400 K. We also use photothermal (PT) technique to obtain the thermal conductivity of the films at room temperature and estimate the thermoelectric figure of merit (ZT). The experimental results suggest that the surface-bound small molecules could serve as a beneficial component to build nanocrystal-based thermoelectric devices operating at low temperature.

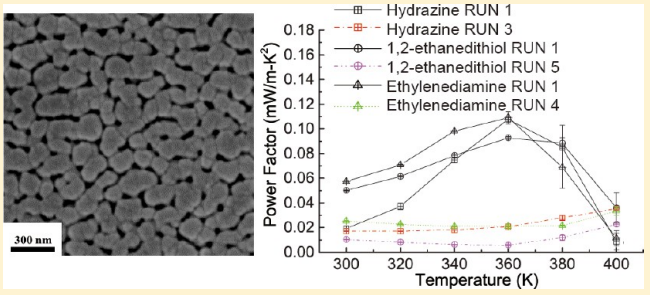

KEYWORDS: *Ligand, nanocrystals, dip coating, hydrazine, 1,2-ethanedithiol, ethylenediamine, thermoelectric, nanocomposite*

Nanocrystal assemblies are considered as a novel type of condensed matter since its behavior depends both on the properties of the individual building blocks and on the many-body exchange interactions. Recent studies of the self-assembled nanocrystal thin films have suggested that they could demonstrate great potential for electronic, thermology, and optoelectronic applications.[1] Notably, because of high surface-to-volume ratio, the surface of the nanocrystal in the self-assembled thin films could have a big influence on physical properties including electron transport, catalysis, magnetism, and so forth. Surfactant molecules, which are widely used in the growth of nanocrystals, could benefit the size control during nanocrystal growth and help to guide the self-assembly toward a more complicated structure;[2,3] However, they could also set a hurdle for charge transport and thus limit the performance of the self-assembled nanocrystal thin film based devices.[4,5]

In this report, we study the thermoelectric property of the Ag_2Te nanocrystal films capped with different molecules. Ag_2Te is chosen as a model system as it possess many advantages such as high electron mobility and low thermal conductivity[6−9] for potential thermoelectric applications.[10,11] In addition, we limit our studies to short-chain molecules such as hydrazine, 1,2-ethanedithiol and ethylenediamine as (1) they have different binding affinity to nanocrystal surface that could alternate the carrier concentration in the nanocrystal thin films[12−14] and (2) they will minimize the blocking of electron transport (compared to the long-chain organic ligands) to maintain a high the electrical conductivity. Of course, this high electron conductivity could also be accompanied by a slight increase in thermal conductivity.[15,16]

To fabricate self-assembled Ag_2Te nanocrystal thin film capped with different surface molecules, we start from the synthesis of Ag_2Te nanocrystals using a recipe modified from the literature by rapid injecting trioctylphosphine-telluride (TOP-Te) solution into a mixture of silver-dodecanethiol and 4-*tert*-butyltoluene.[17] Tellurium (powder, 99.8%), hexane (98.5%), 4-*tert*-butyltoluene (95%), and 1-dodecanethiol (>98%) were purchased from Sigma-Aldrich. Silver nitrate ($AgNO_3$, 99.9%) was purchased from Alfa-Aesar and trioctylphosphine (TOP, 97%) was purchased from Strem Chemicals. All the chemicals are used as received. The synthesis is carried out in a standard Schlenk line protected by nitrogen. In a typical process, 0.364 g of $AgNO_3$ is dissolved in 80 mL of deionized water by ultrasonication. Meanwhile, the solution containing 80 mL fo 4-*tert*-butyltoluene and 1.28 mL of 1-

Received: January 21, 2015
Revised: May 4, 2015
Published: May 22, 2015

DOI: 10.1021/acs.nanolett.5b00255
Nano Lett. 2015, 15, 3748−3756

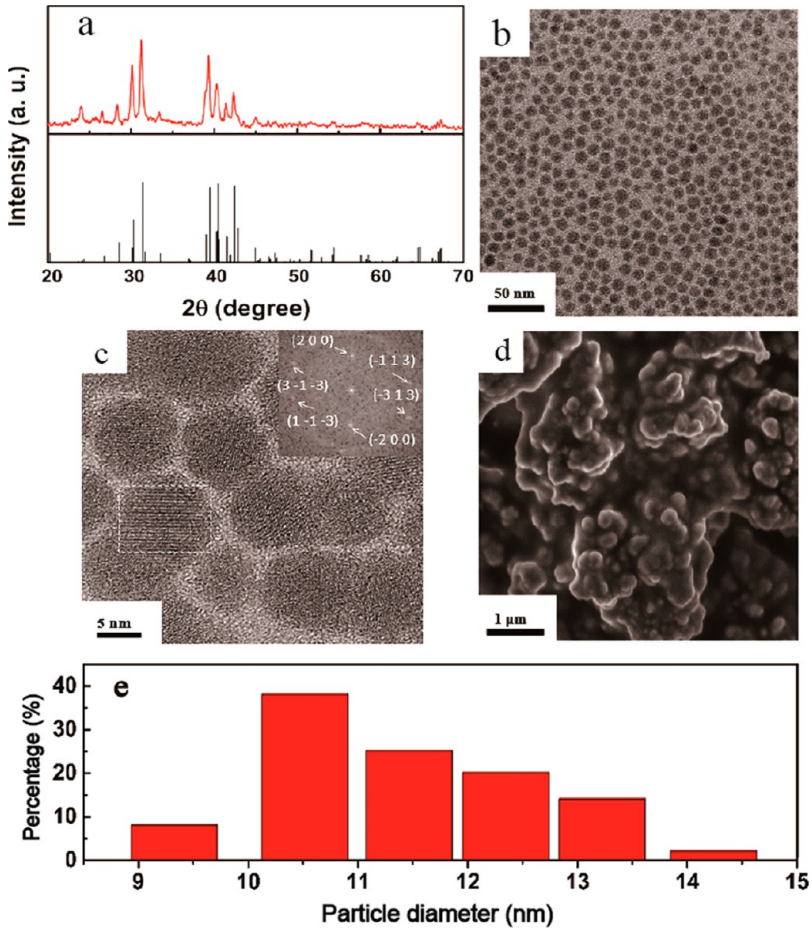

Figure 1. (a) The XRD pattern of Ag_2Te nanocrystals. The red curve is the XRD spectrum of Ag_2Te we synthesized and the black lines below are the peak positions indicated from the standard XRD spectrum of Ag_2Te (JCPDS No. 65-1104). (b) The low-magnification TEM image of the Ag_2Te nanocrystals with an average diameter of 12 ± 3 nm. (c) The HRTEM image of the Ag_2Te nanocrystals. Inset is the FFT of the Ag_2Te region indicated by the white dashed line. (d) The SEM image of Ag_2Te film on glass substrate obtained by direct dip coating without removing 1-dodecanethiol. (e) The diameter distribution histogram of the as-synthesized Ag_2Te nanocrystals.

dodecanethiol is slowly added into the silver nitrate solution with vigorous mixing. After stirring the mixture for 2.5 h, the organic phase (Ag precursor solution) is transferred into a three-neck flask. The flask is purged with nitrogen and heated to 140 °C. In a separate flask, 0.75 M of TOP-Te solution is prepared by dissolving 4.79 g of Te in 50 mL of TOP at 60 °C until the color of the solution present clear yellow. With the fast injection of the 3 mL of 0.75 M TOP-Te into the Ag precursor solution, the color of the solution immediately turned from milk white to dark. The reaction is maintained at 140 °C for 24 h. After that, the reaction is quenched in cool water bath and 6 mL of hexane is added into the solution. The solution is centrifuged three times at 4600 rpm for 6 min to collect the Ag_2Te. The first centrifuge is mainly for removing any large aggregates. During the second and third time centrifuge, 40 mL of ethanol is added as antisolvent to clean and collect the Ag_2Te nanocrystals.

X-ray diffraction (XRD) and transmission electron microscope (TEM) are used to identify the composition, crystal structures, and the size of the products. The XRD pattern (Figure 1a, red curve) clearly demonstrates the pure composition of Hessite phase Ag_2Te (JCPDS No. 65-1104). The low-magnification TEM study (Figure 1b) shows uniform-sized nanocrystals with an average diameter of 12 ± 3 nm (Figure 1e). High-resolution TEM (HRTEM, Figure 1c) of individual nanocrystals further confirms that the products are single crystal Ag_2Te nanocrystals and the fast Fourier transform pattern (inset, Figure 1c) clearly shows the diffraction spots that can agree well with the peaks observed in the XRD pattern. Figure 1d shows the scanning electron microscope (SEM) image of the nanocrystal thin film through direct dip coating of glass substrates into the purified Ag_2Te nanocrystal solution. Notably, the nanocrystals are still capped with nonconductive long-chain dodecanethiol surfactant molecules and no ligand exchange reaction has been performed on the nanocrystals. The SEM image clearly shows a rough surface containing large domains from the nanocrystals clustered together.

After the synthesis, the self-assembled Ag_2Te nanocrystal thin films are fabricated by a layer-by-layer (LBL) dip-coating procedure to investigate the impact of surface-bound small molecules on the electrical and thermal properties of the Ag_2Te nanocrystal thin film. All work of the dip-coating process is performed in a nitrogen glovebox with oxygen level lower than 0.1 ppm. On the basis of the coating method reported in our previous paper,[18] we use different small molecules to replace the capping surfactant (1-dodecanethiol) on the surface of the nanocrystals. We choose hydrazine, 1,2-ethanedithiol, and ethylenediamine as model systems because these molecules have very similar structures but different functional group. The size effects of the surface molecules can be minimized, so we

DOI: 10.1021/acs.nanolett.5b00255
Nano Lett. 2015, 15, 3748−3756

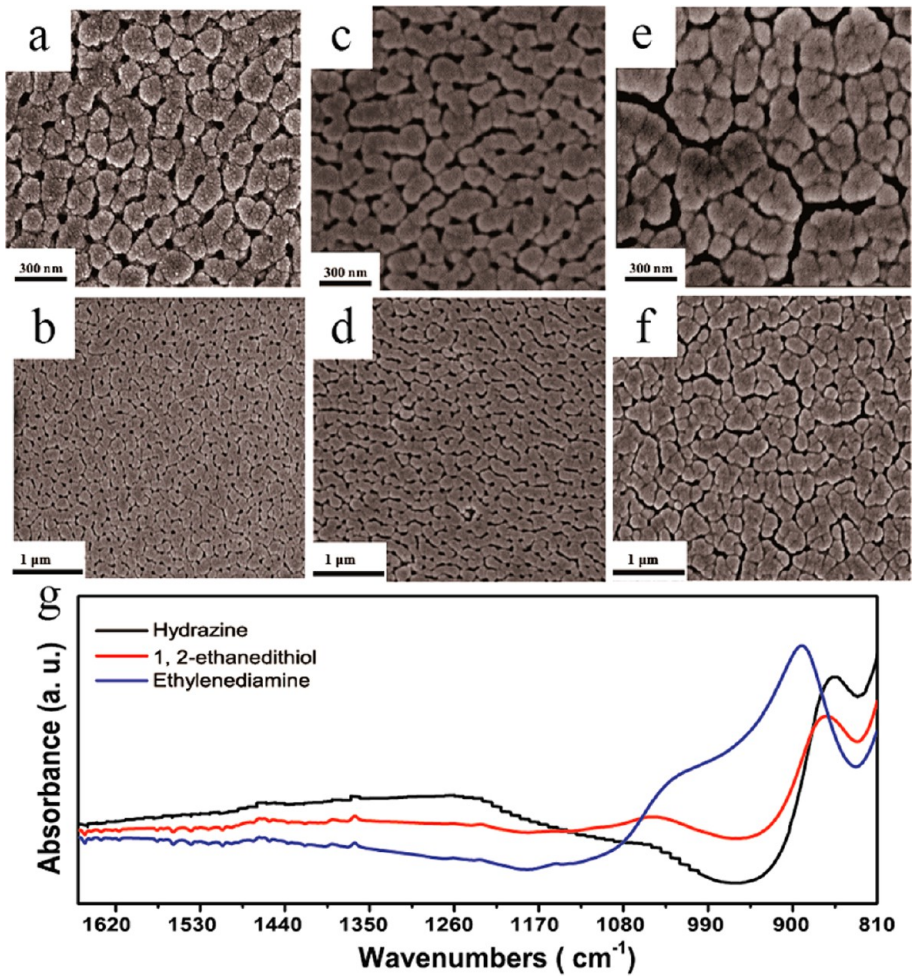

Figure 2. SEM images of Ag_2Te nanocrystal films dip-coated with different small molecules in different magnification: (a,b) hydrazine, (c,d) 1,2-ethanedithiol, and (e,f) ethylenediamine. (g) FTIR spectra of the nanocrystal films containing different small molecules.

have fewer concerns regarding the impacts of the interparticle distance. In addition, these molecules have recently been tested as the capping ligands for nanocrystal-based solar cells,[19,20] which could serve as references in our studies. We have also tried methylamine and benzene-1,3-dithiol as capping ligands. But these two molecules cannot yield a smoothly film based on the same condition, which makes the studies less meaningful.

In a typical coating process, hydrazine (N_2H_4, 99.8%), 1,2-ethanedithiol ($C_2S_2H_6$, 98+%), ethylenediamine ($C_2N_2H_8$, 99%), chloroform (anhydrous, 99+%), and acetonitrile (anhydrous, 99.8%) were purchased from Sigma-Aldrich and used without further purification. The nanocrystal coating solution is prepared by suspending the Ag_2Te nanocrystals in chloroform. Small molecule solutions (0.1 M) of hydrazine, 1,2-ethanedithiol, and ethylenediamine are prepared by mixing the suitable amount of small molecule reagents with anhydrous acetonitrile separately. During the coating process, the glass substrates are first dipped into the Ag_2Te nanocrystal solution, and then they are carefully taken out and dried naturally. After that, the glass substrates are slowly dipped into 0.1 M small molecule solution to exchange the capping surfactant on the surface of nanocrystals. Finally, the substrates are carefully soaked in the anhydrous acetonitrile to remove excessive small molecules from the second step and allowed naturally. This process is repeated until a uniform nanocrystal film with proper thickness is obtained.

The SEM images (Figure 2a–f) show the surface morphologies of the films as a result after the ligand exchange reactions with different small molecules, which could help the nanocrystals to self-assemble into complex patterns.[21] Interestingly, there is no significant difference among the surface morphologies observed from the films being treated with different small molecules. Figure 2g is the Fourier transform infrared spectroscopy (FTIR) image of the different ligands treated films. The peak at 860 cm^{-1} is the characteristic adsorption peak of the $-NH_2$ twisting vibration of the hydrazine-functionalized film (Figure 2g, black curve). The FTIR spectra of 1,2-ethanedithiol-functionalized film has strong C–S stretching vibrations peak at 870 cm^{-1} (Figure 2g, red curve). The FTIR spectra of ethylenediamine-functionalized film have absorption bands at 1150 and 892 cm^{-1} and correspond to the C–N stretching vibration and $-NH_2$ twisting vibration, respectively (Figure 2g, blue curve). The appearance of the peaks proves the successful ligand exchange in the nanocrystal films.

In order to investigate the impact of different surface-bound small molecules on the electrical and thermal properties of Ag_2Te nanocrystal thin films, we have investigated their temperature-dependent Seebeck coefficient and electrical conductivity under vacuum multiple times between by ramping up the temperature from 300 to 400 K, and the results are shown in Figure 3. The Seebeck coefficient is measured by

DOI: 10.1021/acs.nanolett.5b00255
Nano Lett. 2015, 15, 3748–3756

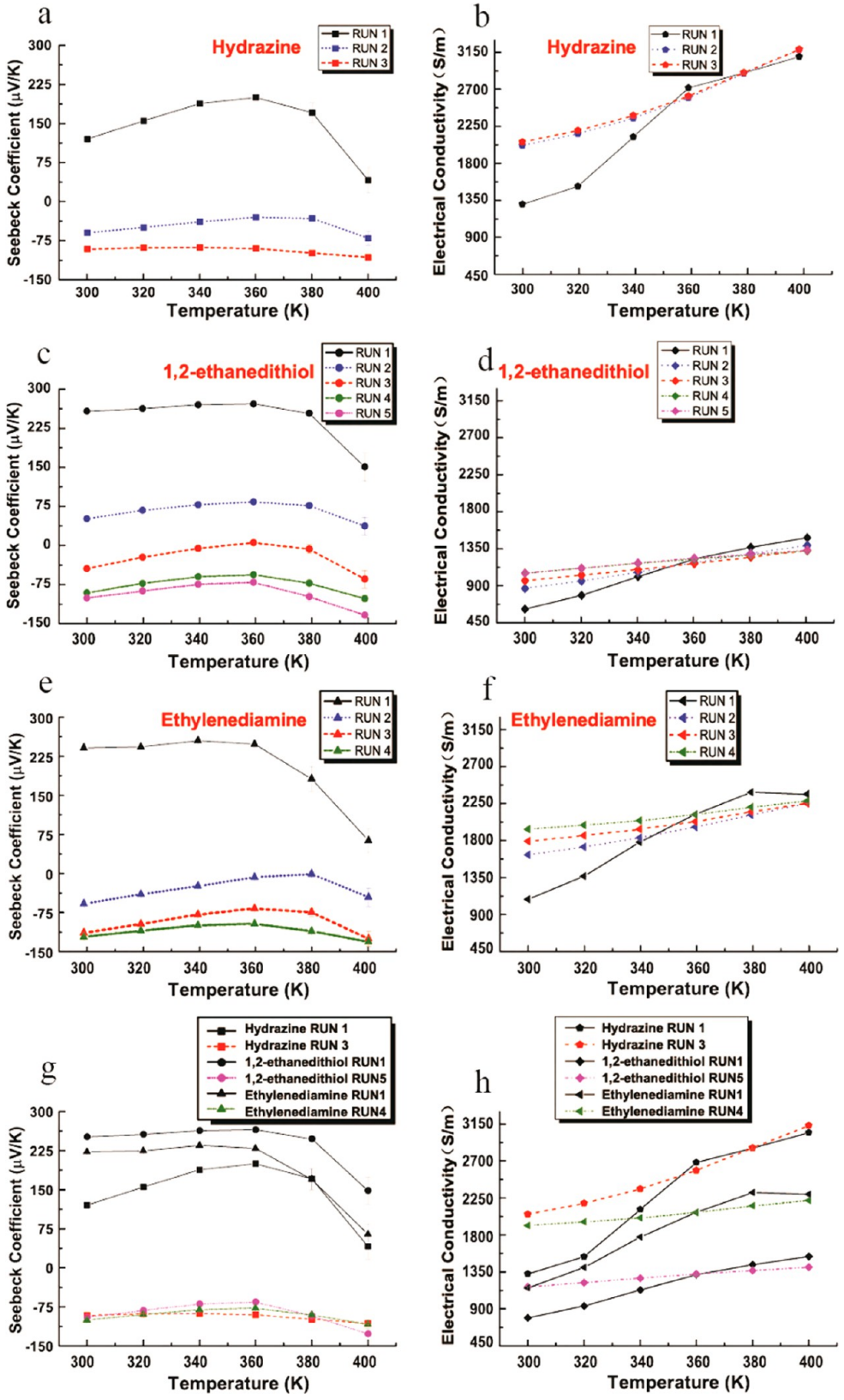

Figure 3. Seebeck coefficient and electric conductivity of nanocrystal thin films with (a,b) hydrazine, (c,d) 1,2-ethanedithiol, and (e,f) ethylenediamine. (g,h) Comparison the results of the first test round and the final test round. Measurements are performed under identical condition under vacuum between 300 and 400 K with same ramp up speed in heating.

bridging the film substrate between a heater and heat sink and testing the voltage and temperature difference between the hot and the cold sides with a maximum temperature fluctuation of ±0.2 K and a voltage resolution of 50 nV. The electrical conductivity is measured through a standard four-probe method with a maximum temperature fluctuation of ±2 K.

DOI: 10.1021/acs.nanolett.5b00255
Nano Lett. 2015, 15, 3748−3756

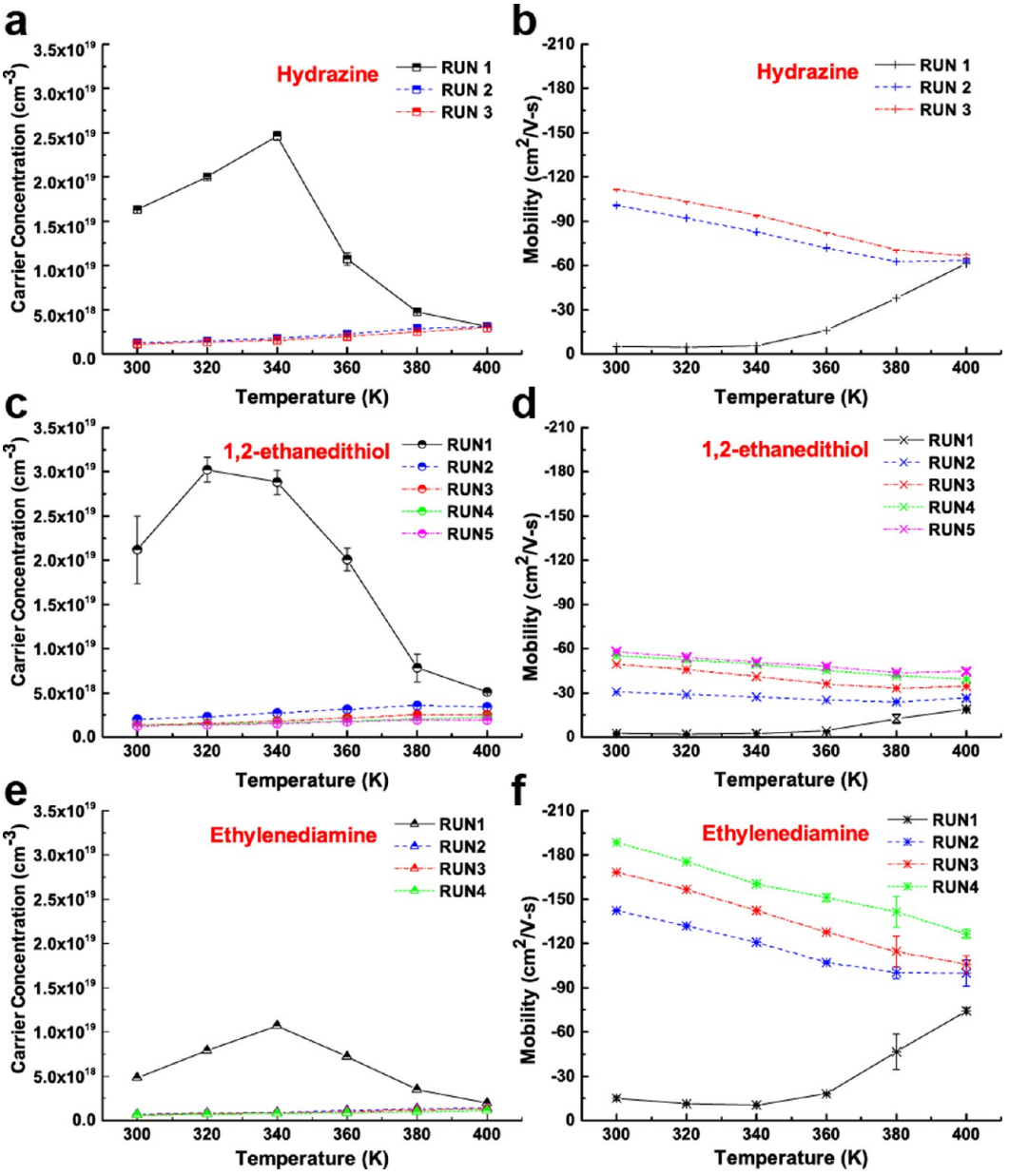

Figure 4. Carrier concentration and mobility of the nanocrystal thin films with (a,b) hydrazine, (c,d) 1,2-ethanedithiol, and (e,f) ethylenediamine.

Figure 3a,b shows the Seebeck coefficient and electrical conductivity of hydrazine-bound nanocrystal thin film. The different colors of the different curves represent different tests. For the first time running, the film shows a positive Seebeck coefficient (black curve, Figure 3a), indicating the nanocrystal thin film has a p-type nature with the maximum values achieved around 360 K. The electrical conductivity (black curve, Figure 3b), however, keeps increasing even over 360 K. For the following tests, we cool down the samples in the test vacuum chamber naturally and repeat the test while ramping up the temperature. The electrical conductivity (blue and red curves, Figure 3b) still shows an increasing trend, but there is no obvious difference between the values in Test Round 2 (blue curve, Figure 3b) and Test Round 3 (red curve, Figure 3b). Interestingly, the Seebeck coefficient shows a significant change from p-type (positive Seebeck coefficient) to n-type (negative Seebeck coefficient) in the Test Round 2 (blue curve, Figure 3a), indicating the dominant carriers in the nanocrystal film change from holes to electrons. In the Test Round 3 (red curve, Figure 3a), the Seebeck coefficient settles and does not show a significant change within the test temperature range. Similar tests are also performed the nanocrystal thin films capped with 1,2-ethanedithiol (Figure 3c,d) and ethylenediamine (Figure 3e,f) and both show similar trend change in the Seebeck coefficient and the electric conductivity. The difference is that it takes more test rounds for the thin film samples capped with 1,2-ethanedithiol (five test rounds) and with ethylenediamine (four test rounds) to settle. The results of the first and the last tests from thin films capped with different small molecules are shown in Figure 3g,h.

Analysis of the results reveals some interesting points: (1) The hydrazine treated film has the lowest Seebeck coefficient value while the highest electric conductivity at the beginning. The 1,2-ethanedithiol treated film, however, has the highest Seebeck coefficient value and the lowest electric conductivity. The ethylenediamine treated film has the values in between. It

DOI: 10.1021/acs.nanolett.5b00255
Nano Lett. 2015, 15, 3748−3756

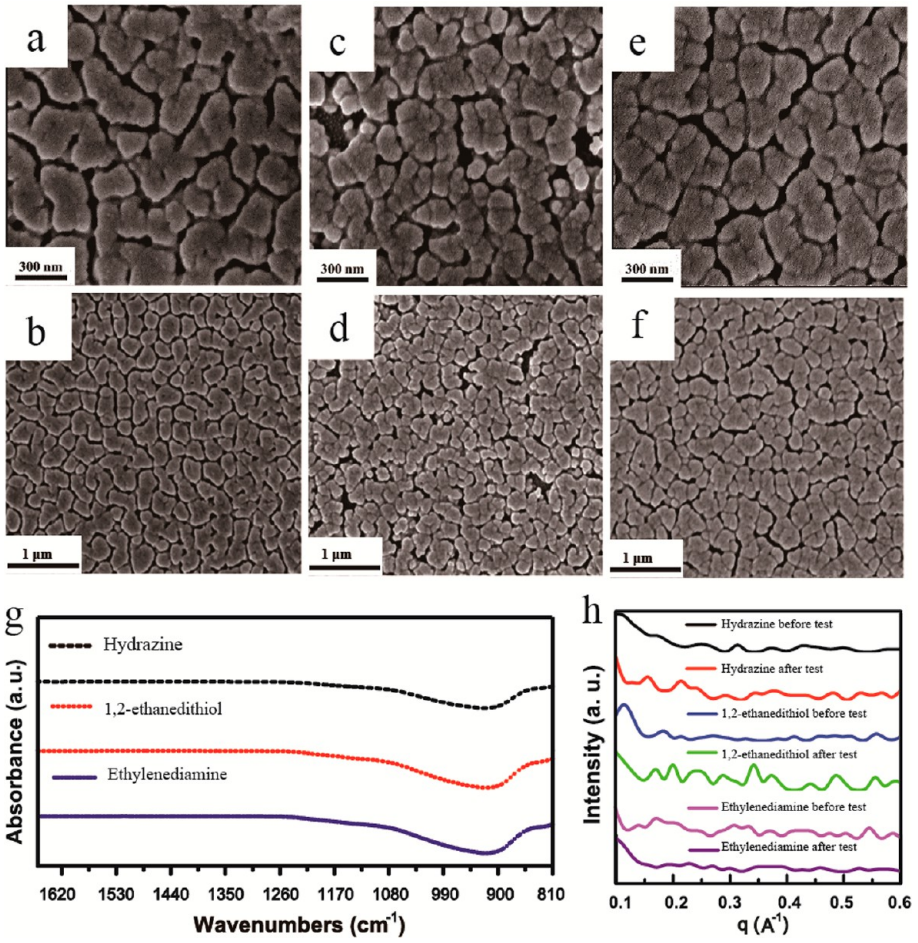

Figure 5. SEM images of Ag_2Te nanocrystal films dip-coated with different small molecules in different magnification after the multiple test rounds: (a,b) hydrazine, (c,d) 1,2-ethanedithiol, and (e,f) ethylenediamine. (g) FTIR spectra of the nanocrystal films containing different small molecules after the multiple test rounds. (h) The small-angle X-ray scattering patterns of Ag_2Te nanocrystal thin films capped with different ligands before and after the multiple test rounds.

can be attributed to the fact that hydrazine has the strongest affinity to attach to the electron deficient metal atoms on the nanocrystal surface than the other two ligands.[22] In addition, hydrazine also does not contain any carbon or C−H bond, meaning there will be less dielectric barriers in the nanocrystal film. It has been reported that different kinds of ligands can lead to different barrier height and width which play the key roles in the evolution of the band structure and transport phenomena.[1] (2) After several cycles of the test, all the films have more or less similar negative Seebeck coefficient. We believe this is an indication that the initial positive Seebeck coefficients observed in all three films are resulting from the small molecule binding. After several cycles of test by heating up the films in vacuum, the surface-bound small molecules are "vaporized" from the nanocrystal surface, which leaves nearly "naked" nanocrystals in the thin films, thus all the films finally show similar Seebeck coefficient as the intrinsic property of the nanocrystals. (3) Under the same test condition, it takes three test rounds, five test rounds, and four test rounds for hydrazine, 1,2-ethanedithiol, and ethylenediamine capped film to reach the similar negative Seebeck coefficient and settle the electrical conductivity, which may indicate that the bond strength between the small molecules and the Ag_2Te is 1,2-ethanedithiol > ethylenediamine > hydrazine, as all three small molecules will form covalent bonds on Ag_2Te surface but the 1,2-ethanedithiol is more likely to form the strongest bond.[16]

To gain more insight into the electrical properties of the nanocrystal thin films capped with different small molecules, Hall effect measurements have been performed to look at the carrier concentration and carrier mobility (Figure 4). We repeat the tests and run the same test cycles under identical condition like what we have done for the Seebeck coefficient and the electric conductivity tests. Figure 4a,c,e are the test results on the carrier concentration and Figure 4b,d,e are the test results on the carrier mobility. The results show the following several key features: (1) In all the films, carrier concentrations (Figure 4a, c, and e) increase and then decrease with increasing test temperature for the first test round. After that, the carrier concentrations in every film with different capping small molecules have little change with the temperature and all show lower carrier concentration compared to the first test rounds. This, combined with our previous tests on the Seebeck coefficient and the electrical conductivity test, further suggest that the small molecules create p-type doping effect for Ag_2Te nanocrystals. (2) In all the films, the absolute values of the carrier mobility (Figure 4b,d,f) increase with increasing test temperature for the first test round. After that, the absolute values of the carrier mobility keep increase after every test round, but overall they show a decreasing trend with increasing

DOI: 10.1021/acs.nanolett.5b00255
Nano Lett. 2015, 15, 3748−3756

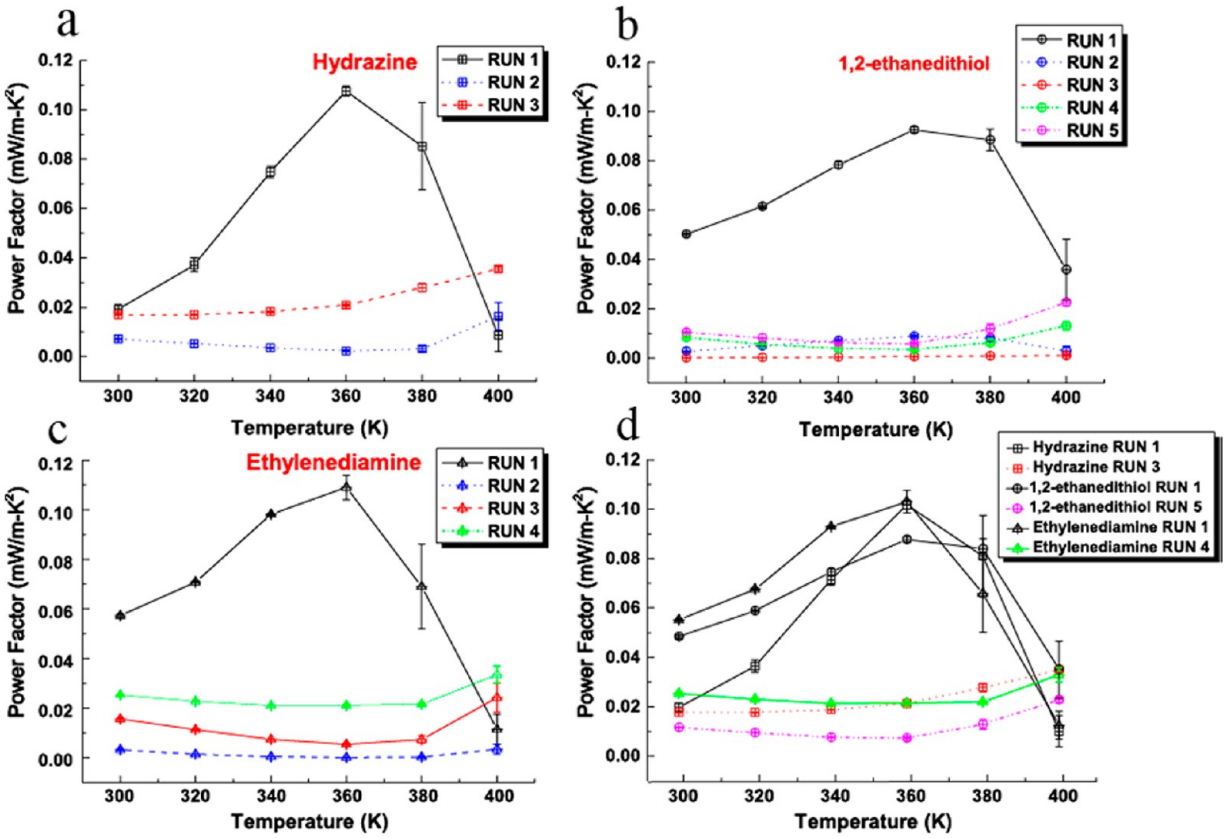

Figure 6. Power factor of nanocrystal thin films capped with (a) hydrazine, (b) 1,2-ethanedithiol, and (c) ethylenediamine. (d) The comparison of all the power factor data obtained from the nanocrystal thin films during the multiple test rounds.

temperature in every film with different capping small molecules. The mobility increase could be explained by the annealing effect in which the small molecules are vaporized gradually and the interparticle distance gets smaller to minimize the charge hopping. The decreasing trend of mobility with increasing temperature after the first test round also agrees with the expected behavior from Ag_2Te that typically shows as a n-type narrow bandgap semiconductor existing in the monoclinic phase.[6]

To confirm our hypothesis and further understand what has happened during the multiple test rounds, we have performed SEM, FTIR, and small-angle X-ray scattering on the nanocrystal thin films and compared the results before and after the test. By comparing the SEM images of the thin films after the tests (Figure 5a–f) and those of the thin film before the tests (Figure 2a-f), we do not see a dramatic change in the morphology or surface roughness. However, the FTIR studies (Figure 5g) clearly show no signature absorption peaks visible after the tests as comparing with the FTIR patterns shown in Figure 2g, indicating the surface-bound small molecules have been "vaporized" from the nanocrystal surface after the multiple rounds of tests. From the small-angle X-ray scattering studies (Figure 5h), we can calculate the interparticle spacing. For the hydrazine-capped thin film, the interparticle distance is ~0.72 nm before the tests and ~0.59 nm after the tests. For the 1,2-ethanedithiol-capped thin film, the interparticle distance is ~0.73 nm before the tests and ~0.51 nm after the tests. For the ethylenediamine-capped thin film, the interparticle distance is ~0.61 nm before the tests and ~0.45 nm after the tests. The decrease in the interparticle distance suggests the elimination of the surface-bound small molecules, which also supports the conclusion drawn from the FTIR studies (Figure 5g) and our hypothesis.

On the basis of the measurement results from the Seebeck coefficients and the electrical conductivity, the corresponding power factors of the three types of Ag_2Te nanocrystal thin films with different surface-bound small molecules are plotted in Figure 6 as well as their evolution as the small molecules leaving the nanocrystal surface. From the comparison results in Figure 6d, we can clearly see that the nanocrystal thin films with small molecules possess a much higher power factor that can reach the maximum value of 0.1 mW/m-K^2 at 360 K. When the small molecules are "vaporizing" from the nanocrystal surface, the power factors start dropping in every type of nanocrystal thin films, which may be related to the dramatically lowered carrier concentration as demonstrated by the Hall measurement results (Figure 4).

We also take an initial step to look at the thermal transport property of the nanocrystal thin films at room temperature using photothermal (PT) technique with multilayer film model[23−26] shown in Figure 7. During the PT experiment, all

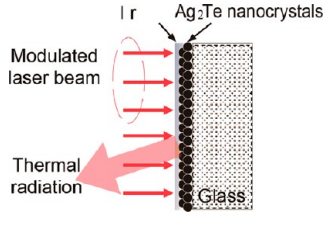

Figure 7. Principle of the photothermal experiment.

DOI: 10.1021/acs.nanolett.5b00255
Nano Lett. 2015, 15, 3748−3756

Table 1. Summary of the Fitted Thermal Conductivities Values and Calculated Room Temperature ZT (ZT_{RT}) for Ag_2Te Nanocrystal Thin Film Samples.[a]

sample	with small molecules	thermal conductivity k at room temperature (W/m·K) ± 5%		ZT_{RT}	ZT_{max}
		phase-shift	amplitude		
hydrazine	no	0.095 ± 0.005	0.127 ± 0.006	0.054	0.15
	yes	0.084 ± 0.004	0.088 ± 0.004	0.071	0.459
1,2-ethanedithiol	no	0.047 ± 0.002	0.052 ± 0.003	0.067	0.204
	yes	0.045 ± 0.002	0.042 ± 0.002	0.320	0.712
ethylenediamine	no	0.031 ± 0.002	0.024 ± 0.001	0.194	0.426
	yes	0.095 ± 0.005	0.086 ± 0.004	0.190	0.417

[a]The ZT_{max} values are calculated by assuming that the thermal conductivity stays the same as room temperature and the molecules don't vaporize.

Ag_2Te nanocrystal thin films are sputter-coated with 60 nm iridium (Ir) on top. A diode laser (809 nm, BWTek) is modulated by a function generator (DS345) and then applied to the Ir layer, which works as a heat source to raise the temperature of the layers below. Meanwhile, the heat energy will both radiate to environment and transfer along the cross plane direction of layers. The response and the intensity of the resulting radiation are closely relative to thermal properties of the layers beneath. The radiation signal from the Ir layer is reflected by two paraboloidal mirrors and then focused on an infrared detector (J15D12, Judson Technology). The reflection of laser beam will be filtered by placing Germanium (Ge) window in front of the detector. The collected signal is transferred to a preamplifier and then the AC component is selected by a lock-in amplifier (SR830). Data acquisition is accomplished by a computer with a lab-designed program.

Considering that the thermal diffusion length in the gas and the target layer is much smaller than the diameter of the laser beam when the laser focal spot (0.7 × 1.4 mm^2) is large enough, the PT experiment can be simplified as a one-dimensional cross-plane heat transfer model for describing temperature distribution and evolution. For an N-layers model, the governing equation for 1D thermal diffusion problem in layer i can be expressed as

$$\frac{\partial^2\theta_i}{\partial x^2} = \frac{1}{\alpha_i}\frac{\partial\theta_i}{\partial t} - \frac{\beta_i I_0}{2k_i}\exp\left(\sum_{m=i+1}^{N} -\beta_m L_m\right) \times e^{\beta_i(x-l_i)}(1 + e^{j\omega t}) \quad (1)$$

where $\theta_i = T_i - T_{amb}$, T_i is the modified temperature of target layer i, and T_{amb} is the ambient temperature. ω is the modulated angular frequency ($2\pi f$). The thickness of layer i is represented as L_i and other thermophysical properties include thermal conductivity k_i, specific heat $C_{p,i}$, thermal diffusivity α_i, the thermal diffusion length $\mu_i = (\alpha_i/\pi f)^{1/2}$, and optical absorption coefficient β_i. The solution θ_i to eq 1 is composed of the transient component $\theta_{i,t}$, the steady DC component $\bar{\theta}_{i,s}$ and the steady AC component $\tilde{\theta}_{i,s}$. Only the AC component $\tilde{\theta}_{i,s}$ will be collected for further evaluation and data processing. The general solution of $\tilde{\theta}_{i,s}$ can be expressed as the following equation with the details of parameters A_i, B_i, E_i, and calculations described in ref 21.

$$\tilde{\theta}_{i,s} = [A_i e^{\sigma_i(x-l_i)} + B_i e^{-\sigma_i(x-l_i)} - E_i e^{\beta_i(x-l_i)}]e^{j\omega t} \quad (2)$$

In our test, the PT measurements for the nanocrystal thin films are conducted over a large frequency ranging from 17 Hz to 20 kHz in the open air at the room temperature. The phase shift between the thermal radiation and the modulated laser and the amplitude of radiation signal are parameters for calculating thermo-physical properties. The system is calibrated before the measurement, and the systematic phase shift and amplitude can be excluded from the experiment data during data preprocessing.

For experimental data processing based on phase shift method, the preprocessed data at each frequency is calculated with $\phi_f = \phi_{raw,f} - \phi_{cal,f}$, where $\phi_{raw,f}$ and $\phi_{cal,f}$ are raw data and calibration data, respectively, at each frequency. The curve of ϕ_f against the frequency is fitted with the lab-developed programming code according to the physics principle. An overall thermal resistance R is thus obtained from the best-fitted curve that is composed of thermal resistance for conduction in Ag_2Te layer R_{cond,Ag_2Te} and thermal contact resistance R''_{tc} at interfaces. Because the thickness of the Ag_2Te layer is very thin, R_{cond,Ag_2Te} has the same order of magnitude as R''_{tc}. Meanwhile the Ag_2Te nanocrystals may not highly compact and the surface is a little coarse which increases R''_{tc} at the interfaces. It is hard to distinguish R_{cond,Ag_2Te} from the overall thermal resistance. Therefore, an overall thermal conductivity $k = R/L$ is employed to represent the thermal properties of Ag_2Te nanocrystals. For experimental data processing based on amplitude method,[27] the normalized amplitude is given by $A_{nor,f} = (A_{raw,f}\cdot\sqrt{f})/A_{cal,f}$ at each frequency. Similar to the process of phase shift data, the fitting program is run to fit the shape of variation of $A_{nor,f}$ against frequency and gives out an overall thermal conductivity for each sample. The overall thermal conductivities for all samples based on two fitting methods are summarized in Table 1, which shows negligible discrepancy between two fitting methods for the results obtained in most samples.

Analysis of the room-temperature thermal conductivity data show the following interesting insights of our nanocrystal thin films. (1) All the films have extremely low thermal conductivity. (2) The nanocrystal thin film with the surface-bound small molecules generally have slightly lower thermal conductivity as the results of enhanced phonon scattering from surface molecules.[16] We also believe that the possible increase in the grain size due to the sintering effect during the sequential tests, as indicated by the TEM studies of the cross sections of the nanocrystal thin film (not shown), could also lead to the higher thermal conductivity in the nanocrystal films after the surface ligands vaporize. The only exception is ethylenediamine-capped nanocrystal thin films, which show a higher thermal conductivity. The exact reason is unclear and definitely worth further experimental and theoretical investigation on the electronic structures of Ag_2Te nanocrystal capped with ethylenediamine. (3) According to the result from the thermal conductivity in room temperature, we can roughly estimate the ZT value, which give a room temperature ZT of 0.32 for the

DOI: 10.1021/acs.nanolett.5b00255
Nano Lett. 2015, 15, 3748−3756

Ag_2Te nanocrystal capped with 1,2-ethanedithiol, mainly due to its low thermal conductivity. Notably, if we assume the thermal conductivity value remains the same for the entire temperature range (300−400 K) and the surface-bound molecules (1,2-ethanedithiol) can stay permanently, a maximum ZT of 0.712 may be achievable. At the same time, the ZT for uncapped Ag_2Te nanocrystal films ranges between 0.054 and 0.194.

The room-temperature power factors of our Ag_2Te nanocrystal films are relatively lower than the previously reported studies on the carbon nanotube-Ag_2Te system[28] and pure Ag_2Te nanowire system developed in our group;[29] however, due to the extremely low thermal conductivity observed in our nanocrystal films the room-temperature ZT of our Ag_2Te nanocrystal films are comparable or even slightly better than the carbon nanotube-Ag_2Te system[28] and pure Ag_2Te nanowire system.[29] A significant advantage for the nanocrystal thin films presented here is that no high-temperature annealing or pressed sintering is needed, which could enable many potential applications when using ligand-capped nanocrystals as for printable or sprayable molecular inks for the fabrication of thermoelectric devices on polymer-based fabrics. However, due to the vaporization of the small ligand molecules, the stability of the electrical and thermal properties at higher temperature raises a serious concern. In order to realize this great potential of using colloidal nanocrystal as "molecular inks", it will require the further optimizations in designing a nanocrystal-molecule system with proper band alignment to increase the carrier concentration while at the same time a better surface chemistry to ensure the stability of organic molecules on the nanocrystal surface at elevated temperature through the combination of theoretical electronic structure calculation and surface chemistry experiments.

In conclusion, we have performed a systematic study on the impact of several types of surface-bound small molecules on the thermoelectric properties of the Ag_2Te nanocrystal thin film made by dip-coating method. By analyzing the experimental results, we can reach the conclusion that the incorporation of small molecules into the certain nanocrystal thin film could potentially benefit to achieve a higher power factor and a lower thermal conductivity, leading to an enhanced performance near room temperature.

AUTHOR INFORMATION

Author Contributions

All authors have given approval to the final version of the manuscript.

Notes

The authors declare no competing financial interest.

ACKNOWLEDGMENTS

Y.S. thanks the support from China Scholarship Council for the exchange study at Purdue University. Y.W. thanks the support from US Air Force Office of Scientific Research (Award Number FA9550-12-1-0061). Y.W. and X.W. also thank the partial support from the Accelerating Collaboration in Research Initiative of the College of Engineering at Iowa State University.

REFERENCES

(1) Talapin, D. V.; Lee, J.; Kovalenko, M. V.; Shevchenko, E. V. *Chem. Rev.* **2010**, *110*, 389−458.
(2) Palmer, R. E.; Wilde, G. *Nanostructured Materials*, 1st ed.; Elsevier Ltd.: London, 2009.
(3) Ortiz, D.; Kohlstedt, K. L.; Nguyen, T. D.; Glotzer, S. C. *Soft Matter* **2014**, *10*, 3541−3552.
(4) Shevchenko, E. V.; Talapin, D. V.; Kotov, N. A.; OBrien, S.; Murray, C. B. *Nature* **2006**, *439*, 55−59.
(5) Cadavid, D.; Ibáñez, M.; Shavel, A.; Dur, O. J.; de la Torrec, M. A. L.; Cabot, A. *J. Mater. Chem. A* **2013**, *1*, 4864−4870.
(6) Gnanadurai, P.; Soundararajan, N.; Sooriamoorthi, C. E. *Phys. Status Solidi* **2003**, *237*, 472−478.
(7) Sahu, A.; Qi, L.; Kang, M. S.; Deng, D.; Norris, D. J. *J. Am. Chem. Soc.* **2011**, *133*, 6509−6512.
(8) Yarema, M.; Pichler, S.; Sytnyk, M.; Seyrkammer, R.; Lechner, R. T.; Fritz-Popovski, G.; Jarzab, D.; Szendrei, K.; Resel, R.; Korovyanko, O.; Loi, M. A.; Paris, O.; Hesser, G.; Heiss, W. *J. Am. Chem. Soc.* **2011**, *5*, 3758−3765.
(9) Li, D.; Xie, H.; Liu, J.; Duan, C. *J. Exp. Nanosci.* **2011**, *6*, 209−216.
(10) Taylor, P. F.; Wood, C. *J. Appl. Phys.* **1961**, *32*, 1.
(11) Guin, S. N.; Chatterjee, A.; Biswas, K. *RSC Adv.* **2014**, *4*, 11811−11815.
(12) Law, M.; Luther, J. M.; Song, Q.; Hughes, B. K.; Perkins, C. L.; Nozik, A. J. *J. Am. Chem. Soc.* **2008**, *130*, 5974−5985.
(13) Jarosz, M. V.; Porter, V. J.; Fisher, B. R.; Kastner, M. A.; Bawendi, M. G. *Phys. Rev. B* **2004**, *70*, 195327.
(14) Kovalenko, M. V.; Scheele, M.; Talapin, D. V. *Science* **2009**, *324*, 1417−1420.
(15) Coe, S.; Woo, W.; Bawendi, M.; Bulovic, V. *Nature* **2002**, *420*, 800−803.
(16) Ong, W.; Rupich, S.; Talapin, D.; McGaughey, A.; Malen, J. *Nat. Mater.* **2013**, *12*, 410−415.
(17) Liu, Y.; Ko, D.; Oh, S.; Gordon, T.; Doan-Nguyen, V.; Paik, T.; Kang, Y.; Ye, X.; Jin, L.; Kagan, C. R.; Murray, C. B. *Chem. Mater.* **2011**, *23*, 4657−4659.
(18) Liang, D.; Yang, H.; Finefrock, S. W.; Wu, Y. *Nano Lett.* **2012**, *12*, 2140−2145.
(19) Luther, J. M.; Law, M.; Song, Q.; Perkins, C. L.; Beard, M. C.; Nozik, A. J. *ACS Nano* **2008**, *2*, 271−280.
(20) Law, M.; Luther, J. M.; Song, Q.; Hughes, B. K.; Perkins, C. L.; Nozik, A. J. *J. Am. Chem. Soc.* **2008**, *130*, 5974−5985.
(21) DeVries, G. A.; Brunnbauer, M.; Hu, Y.; Jackson, A. M.; Long, B.; Neltner, B. T.; Uzun, O.; Wunsch, B. H.; Stellacci, F. *Science* **2007**, *315*, 358−361.
(22) Kovalenko, M. V.; Bodnarchuk, M. I.; Zaumseil, J.; Lee, J.; Talapin, D. V. *J. Am. Chem. Soc.* **2010**, *132*, 10085−10092.
(23) Hu, H.; Wang, X.; Xu, X. *J. Appl. Phys.* **1999**, *86*, 3953−3958.
(24) Wang, T.; Wang, X.; Zhang, Y.; Liu, L.; Xu, L.; Liu, Y.; Zhang, L.; Luo, Z.; Cen, K. *J. Appl. Phys.* **2008**, *104*, 013528.
(25) Chen, X.; He, Y.; Zhao, Y.; Wang, X. *Nanotechnology* **2010**, *21*, 055707.
(26) Xu, Z.; Xu, S.; Tang, X.; Wang, X. *AIP Adv.* **2014**, *4*, 017131.
(27) Xu, S.; Xu, Z.; Starrett, J.; Hayashi, C.; Wang, X. *Polymer* **2014**, *55*, 1845−1853.
(28) Yu, C.; Choi, K.; Yin, L.; Grunlan, J. C. *ACS Appl. Mater. Interfaces* **2014**, *6*, 4940−4946.
(29) Yang, H.; Bahk, J. H.; Day, T.; Mohammed, A. M. S.; Min, B.; Snyder, G. J.; Shakouri, A.; Wu, Y. *Nano Lett.* **2014**, *14*, 5398−5404.

DOI: 10.1021/acs.nanolett.5b00255
Nano Lett. 2015, 15, 3748−3756